
Article:
Li, Wei Li, Kunin, Alice, Matthews, Edward et al. (2016) Photodissociation dynamics of the iodide-uracil (I-U) complex. Journal of Chemical Physics. 044319. ISSN: 1089-7690

https://doi.org/10.1063/1.4959858

Photodissociation dynamics of the iodide-uracil (I^-U) complex

Wei-Li Li[1], Alice Kunin[1], Edward Matthews[2], Naruo Yoshikawa,[2] Caroline E. H. Dessent[2], Daniel M. Neumark[1,3,*]

[1]*Department of Chemistry, University of California, Berkeley, CA 94720, USA.*

[2]*Deparment of Chemistry, University of York, Heslington, York, YO10 5DD, UK.*

[3]*Chemical Sciences Division, Lawrence Berkeley National Laboratory, Berkeley, CA 94702, USA*

E-mail: dneumark@berkeley.edu, caroline.dessent@york.ac.uk

Abstract

Photofragment action spectroscopy and femtosecond time-resolved photoelectron imaging are utilized to probe the dissociation channels in iodide-uracil ($I^-\cdot U$) binary clusters upon photoexcitation. The photofragment action spectra show strong I^- and weak $[U-H]^-$ ion signal upon photoexcitation. The action spectra show two bands for I^- and $[U-H]^-$ production peaking around 4.0 and 4.8 eV. Time-resolved experiments measured the rate of I^- production resulting from excitation of the two bands. At 4.03 eV and 4.72 eV, the photoelectron signal from I^- exhibits rise times of 86 ± 7 ps and 36 ± 3 ps, respectively. Electronic structure calculations indicate that the lower energy band, which encompasses the vertical detachment energy (4.11 eV) of I^-U, corresponds to excitation of a dipole-bound state of the complex, while the higher energy band is primarily a π-π^* excitation on the uracil moiety. Although the nature of the two excited states is very different, the long lifetimes for I^- production suggest that this channel results from internal conversion to the $I^-\cdot U$ ground state followed by evaporation of I^-. This hypothesis was tested by comparing the dissociation rates to Rice-Ramsperger-Kassel-Marcus (RRKM) calculations.

I. INTRODUCTION

High energy radiation is capable of producing free electrons as it passes through matter, and these free electrons can generate large quantities of lower energy secondary electrons.[1] Both primary and secondary electrons can cause damage to DNA in living cells.[1] Extensive studies have shown that free electrons with energy well below the ionization potential of DNA consituents can cause both single- and double-strand breaks in DNA.[2-12] Experimental and theoretical investigations have been performed to understand the underlying DNA damage mechanism at the molecular level. Theoretical studies suggest that cleavage is initiated by electron attachment to one component of the DNA strand to form a transient negative ion, followed by subsequent fragmentation.[13-17] The unoccupied low-lying π^* anti-bonding orbitals of nucleobases and dissociative σ^* orbital of phosphate groups are possible sites of electron capture.[13-16] Experimentally, dissociative electron attachment studies of uracil find that the dominant channel at low collision energy is the production of the deprotonated nucleobase, where the H loss occurs at the nitrogen positions.[18] O-H and P=O/P-O bond breaks are also observed as a result of electron attachment to the phosphate group.[16] We have previously studied electron-nucleobase interactions by photoexcitation of gas phase iodide nucleobase (NB) anions, in which low energy electrons that are photodetached from the iodide are captured by the nucleobase, forming a temporary negative ion whose subsequent dynamics are followed by time-resolved photoelectron spectroscopy.[19-23] In this paper, we characterize the products of this photoexcitation in more detail, focusing primarily on the mechanism by which I^- is formed by ultraviolet excitation of iodide-uracil anions.

In previous work, femtosecond pump-probe experiments based on the following excitation and detection scheme were carried out on $I^-\cdot$uracil ($I^-\cdot U$),[19, 21] $I^-\cdot$thymine ($I^-\cdot T$),[20, 22] and $I^-\cdot$adenine ($I^-\cdot A$) complexes.[23]

$$I^- \cdot NB \xrightarrow{h\nu_{pump}} I \cdot NB^{*-} \xrightarrow{h\nu_{probe}} I \cdot NB + e^- \qquad (1)$$

An ultraviolet pump pulse photexcites the complex, forming a transient I·NB*⁻ species in which neutral iodine is bound to a dipole-bound (DB) or valence-bound (VB) nucleobase anion. This temporary negative anion is photodetached by a near-infrared probe pulse and the resulting photoelectron (PE) spectrum is measured. The PE spectrum enables one to determine if a DB and/or VB nucleobase anion is formed,[24-26] to follow the conversion of a DB anion to a VB anion,[27] and to measure the lifetime of either species with respect to electron loss and other possible decay channels. Experiments on I⁻·U and I⁻·T were performed at pump photon energies in two energy ranges: near 4.0 eV, which is very close to the vertical detachment energy (VDE) of the complexes, and around 4.7 eV, well above the VDE. Excitation at the lower energy range yields both DB and VB anions. The time-evolving spectra suggest that some of the DB states convert to VB states on a timescale of several hundred femtoseconds. At the higher energies, the VB state is formed instantaneously within the time resolution of our experiment (<150 fs), and there is no evidence for a DB state. These short-time electron attachment dynamics have been interpreted with the aid of electronic structure calculations that have considered the energetics and structure of the DB and VB anions.[26, 28-31]

At longer times, the DB and VB features in I⁻·U and I⁻·T exhibit either mono-exponential or bi-exponential decay. One of these decay channels was established to be autodetachment,[19, 20] in which a very low energy electron is emitted from the temporary negative ion created by the pump pulse. However, other channels are energetically accessible:

$$
\begin{aligned}
I \cdot U^{*-} &\rightarrow I + U^{*-} \\
&\rightarrow I^- + U \qquad (2) \\
&\rightarrow HI + [U - H]^-
\end{aligned}
$$

The time-resolve PE imaging (TRPEI) experiments carried out thus far on these complexes used a probe wavelength of 790 nm (1.57 eV), which was sufficiently energetic to photodetach I·U*$^-$ and U*$^-$, but not I$^-$ or the deprotonated [U-H]$^-$ anion, for which the corresponding neutral electron affinities are 3.059 eV[32] and 3.481 eV,[33] respectively. In the current study, we carry out photofragment action spectroscopy on I$^-$·U from 3.6-5.2 eV to determine the yields of I$^-$ and [U-H]$^-$ as a function of UV excitation energy, and thus gaining insight into which of the energetically accessible decay channels are active. We find that the action spectra for both fragments comprise two broad bands with maxima at approximately 4.0 eV and 4.8 eV. Complementary TRPEI experiments at higher probe photon energies have also been carried out at 4.03 and 4.72 eV with the specific goal of time-resolving the appearance of the I$^-$ channel. These long lifetimes suggest that I$^-$ is produced by internal conversion from the excited state I·U*$^-$ created by the pump pulse to the ground I$^-$·U, followed by statistical decay to I$^-$ + U.

II. EXPERIMENTAL METHOD

Photodepletion (absorption) and photofragment action spectra were conducted in a Bruker AmaZon Ion Trap mass spectrometer at the University of York that has been custom-modified for performing laser spectroscopy.[34, 35] The I$^-$·U clusters were generated by electrospraying solutions of uracil and iodide in deionized water (nucleobase solutions were 1x10^{-4} mol/dm^3, mixed with droplets of the t-butyl ammonium iodide (TBAI) at 1x10^{-2} mol/dm^3). All chemicals were

purchased from Sigma Aldrich and used without further purification. The $I^-\cdot U$ clusters were mass-selected and isolated in the instrumental ion-trap prior to laser irradiation. The photofragment ion intensity was then recorded using the normal functions of the mass spectrometer. UV photons for the photofragmentation experiment were produced by a Nd:YAG (Continuum Surelite) pumped optical parametric oscillator (OPO) (Continuum Horizon), producing ~2 mJ across 225-310 nm. The spectral resolution is determined by the laser step size (1 nm or ~0.018 eV in the mid-spectral region) for the action spectra presented here. All spectra are corrected for laser power.

The femtosecond time-resolved photoelectron imaging apparatus at Berkeley has been described in detail previously.[36, 37] $I^-\cdot U$ clusters were produced by thermal desorption of solid uracil (Sigma-Aldrich, ≥99.0%) loaded in an Even-Lavie pulsed valve and then entrained by 40 psig argon carrier gas mixed with iodomethane vapor. The gas mixture was supersonically expanded into vacuum and passed through a ring electrode ionizer for secondary electron attachment to form the binary cluster anions. The anionic clusters were then perpendicularly extracted and analyzed using a Wiley-McLaren time-of-flight mass spectrometer. Clusters of interest were isolated by a mass gate before interacting with the pump and probe laser beams. Two pump-probe schemes were used in these experiments. Near the VDE, the pump pulse (308 nm, 4.03 eV, 5 μJ/pulse) was generated from a 1 kHz, 2.0 mJ 790 nm pulse (KM Labs Griffin Oscillator and Dragon Amplifier) by frequency doubling the second harmonic signal of an optical parametric amplifier (OPA) (Light Conversion TOPAS-C). The probe pulse (344 nm, 3.61 eV, 8 μJ/pulse) was formed by combining the residual TOPAS-C signal and the fundamental 790 nm pulse. For excitation well above the VDE, the pump pulse (263 nm, 4.72 eV, 5 μJ/pulse) was produced by frequency tripling the fundamental pulse and the probe (395 nm, 3.15 eV, 80 μJ/pulse) was generated by doubling the fundamental pulse. The cross-correlation of the pump and probe pulses

was less than 150 fs for 308 nm/344 nm and 200 fs for 263 nm/395 nm. After laser interaction, the resulting photoelectrons were extracted and analyzed by velocity map imaging (VMI) onto a position-sensitive microchannel plate detector. The photoelectron kinetic energy (eKE) distributions and photoelectron angular distributions (PADs) were reconstructed from the images using basis-set expansion (BASEX)[38] reconstruction methods.

III. RESULTS

The negative ion electrospray mass spectrum of the mixed I^- + U solution is displayed in Fig. S1.[39] The spectrum is dominated by the I^- ion and the I^-·TBAI salt cluster; the I^-·U cluster signal is weaker but clearly visible. The photodepletion (absorption) spectrum for the I^-·U cluster was obtained across the region from approximately 3.6 eV to 5.2 eV and is shown in Fig. 1a. The spectrum has an onset at approximately 3.75 eV and the first strong absorption band is observed near 4.0 eV, indicating that an excited state of the cluster exists in the region below the VDE of I^-·U of 4.11 eV[19-21], as would be expected for the DBS observed previously.[21] Continuously strong absorption is observed up to approximately 5.2 eV, consistent with significant direct electron detachment from the cluster. Fig. 1b shows the photofragmentation action spectrum of I^-. Similar to the absorption spectrum, the I^- signal has an onset at approximately 3.75 eV. The first strong I^- ion production band is observed with a band maximum at 4.0 eV. Another strong I^- production region lies between 4.2 eV to 5.3 eV, peaking at 4.8 eV. The intensity ratio for 4.0 eV/4.8 eV for I^- is approximately 3:2. The action spectrum of $[U\text{-}H]^-$ is shown in Fig. 1c; the most intense $[U\text{-}H]^-$ photofragment bands occur around 4.0 eV and 4.8 eV, similar to the I^- signal. The intensity ratio at 4.0 eV/4.8 eV for $[U\text{-}H]^-$ is 4:1. The photofragmentation mass spectrum of I^-·U obtained

at 4.78 eV (Fig. S2) shows I^- as the dominant photofragment and $[U-H]^-$ as a minor photofragment. Thus, the dominant cluster photofragmentation process (i.e. excluding electron detachment) is cluster fission: $I^-\cdot U \rightarrow I^- + U$.

To investigate the time-resolved dissociation dynamics, TRPEI spectra were recorded at excitation energies of 4.03 eV and 4.72 eV, near the two band maxima in the photofragment action spectra. Fig. 2 shows representative time-resolved spectra at pump and probe energies of 4.03 eV and 3.61 eV (343 nm), respectively. Three major features are observed in the spectra. The most intense feature A occurs near eKE=0. Its intensity does not obviously change with varying pump-probe delays, and it is attributed to autodetachment resulting from excitation at the pump energy.[19-21] A sharp feature B is observed at eKE= 0.55 ± 0.06 eV. Its intensity at negative delay time, in which the probe pulse arrives before the pump pulse, is zero and increases for positive delays until it reaches a plateau. Based on its kinetic energy and narrow peak width, we can readily assign feature B to photodetachment of I^- by the probe pulse. The contour plot of background-subtracted signal for feature B is shown in Fig. 3. A very weak feature C is observed near 3.5 ± 0.1 eV eKE, and its intensity is also time-dependent. This feature is assigned as photodetachment from the DBS by the probe pulse, which has been examined in detail previously.[21] Although the probe pulse is sufficiently energetic to photodetach the $[U-H]^-$ anion, no evidence for this species is seen in either Fig. 2 or 3.

Fig. 4 shows representative TRPEI spectra at an excitation energy of 4.72 eV and a probe energy of 3.15 eV (395 nm). The pump-only spectrum at -100 ps shows a strong autodetachment peak A near zero-eV eKE (see inset) as well as a peak C around 0.6 eV. Feature C is attributed to the direct detachment of $I^-\cdot U$ by the pump pulse. The time-dependent feature B occurs at slightly

higher kinetic energy than feature A, 0.09 ± 0.02 eV at large positive delay times, and, as in Fig. 2, is readily assigned to detachment of I^- by the probe pulse. Note that the probe energy used in Fig. 2 would have placed feature B directly on top of feature C, where it would be even more difficult to discern since the probe pulse at 343 nm is considerably weaker than that at 395 nm (see Section II). The contour plot of background-subtracted signal for feature B with respect to the most negative delay time is shown in Fig. 5.

IV. ANALYSIS

The photofragment action spectrum for I^- in Fig. 1 shows evidence for two dissociative electronic states of I^-·U at 4.0 eV and 4.8 eV. These transitions can be assigned with the aid of equation of motion coupled cluster singles and doubles (EOM-CCSD) excited states calculations. The anion ground state geometry optimization was first performed at MP2 level with an augmented Dunning basis set aug-cc-pVDZ for C, H, O, N[40] and aug-cc-pVDZ-pp with an expanded basis set with an increased set of diffuse functions for iodide[40-42] (MP2/aug-cc-pVDZ-(pp)). The optimized structure was used in the EOM-CCSD calculation. All calculations were performed using the Gaussian 09 program.[43] Table 1 presents the transition channels, excitation energies, corresponding oscillator strength, and final state configurations. The six electronic transitions with largest oscillator strength are marked bold in Table 1. All the excitation energies are offset by -0.52 eV for comparison with experiment. Three electronic transitions from 4.04 to 4.24 eV correspond to transitions from a *5p* orbital on the iodide anion to form a DBS of the complex. These three channels contribute to the strong absorption band around 4.0 eV. The most intense transition, calculated at 4.77 eV, is the π-π^* transition on the nucleobase. This and two weaker

transitions contribute to the strong absorption band around 4.8 eV. Therefore the lower and higher bands in the I^- action spectrum are primarily from I(*5p*)-DB and π - π* transitions, respectively. The calculation also shows three very weak transitions between 4.5 eV to 4.6 eV corresponding to electron transfer from the I(*5p*) orbital to the π* anti-bonding orbital, i.e. direct formation of the anion VB state by optical excitation.

Table 1. EOM-CCSD calculated transition channels, excitation energies, oscillator strength, and final state configurations. Calculated at the EOM-CCSD/aug-cc-pVTZ-(pp) level of theory

Excitation Energy (eV)	Oscillator strength	Transition Channels	Final States
4.04[a]	**0.0879**	**I(*5p*)-DBO**	**I($5p^5$)U$^-$(DBO^1)**
4.06	**0.0956**	**I(*5p*)-DBO**	**I($5p^5$)U$^-$(DBO^1)**
4.23	**0.1176**	**I(*5p*)-DBO**[b]	**I($5p^5$)U$^-$(DBO^1)**
4.49	0.0011	I(*5p*)- π*	I($5p^5$)U$^-$($\pi^4\pi^{*1}$)
4.56	0.0016	I(*5p*)- π*	I($5p^5$)U$^-$($\pi^4\pi^{*1}$)
4.61	0.0000	I(*5p*)- π*	I($5p^5$)U$^-$($\pi^4\pi^{*1}$)
4.66	**0.0400**	**I(*5p*)-σ***	**I($5p^5$)U$^-$(σ^{*1})**
4.68	**0.0274**	**I(*5p*)-σ***	**I($5p^5$)U$^-$(σ^{*1})**
4.77	**0.3100**	**π – π***	**I$^-$($5p^6$)U($\pi^3\pi^{*1}$)**

[a] All energies are in eV. The tabulated excitation energies are offset by -0.52 eV from the calculated values to facilitate comparison with the experimental data.
[b] dipole-bound orbital (DBO).

We next consider the time-dependent photoelectron signals in Figs. 2-5. The integrated intensity change of feature B at 4.03 eV is fit using Equation 3. The fitting for feature B yields a mono-exponential rise time of 86 ± 7 ps, as shown in Fig. 6. The DBS decays bi-exponentially with time constants of 6 ps and 2800 ps (Fig. S3), which lies within error bars of the previously reported values, 8.5 ps and 2000 ps, from earlier experiments at an excitation energy of 4.00 eV.[21]

$$I(t) = I_0 - \sum_i A_i \cdot \exp(-t/\tau_i) \qquad (3)$$

At 4.72 eV, the intensity integration was performed over the range from 0.02 eV to 0.2 eV, which includes both features A and B since they are partially overlapped. In previous work, the autodetachment feature A exhibited some time-resolved dynamics.[19-21] However, its intrinsic intensity change as a function of time was very minor compared to the total intensity change of features A and B observed in the current experiment. Thus, the major intensity change between 0.02 eV to 0.2 eV is caused by feature B and therefore can be used to represent the dynamics of feature B. The integrated intensity of feature B from 0.02 to 0.2 eV is shown in Fig. 7. This feature also fits well to a mono-exponential rise, but has a faster rise time of 36 ± 3 ps compared to excitation at 4.03 eV.

The long time constants for I^- formation and their drop with increasing pump energy suggest a statistical decay channel; a possible overall mechanism is internal conversion from the excited $I \cdot U^{*-}$ state to a highly vibrationally excited $I^- \cdot U$ ground state that decays to I^- + U. This process should be amenable to a statistical treatment such as RRKM theory.[44, 45] It is thus useful to carry out RRKM calculations of the dissociation rate at the two excitation energies and compare these results with our experimental values.

According to RRKM theory, the microcanonical reaction rate constant $k(E)$ for a given energy depends on the sum of states of the transition state, $G(E - E_0)$, and the density of states of the reactant, $N(E)$, as expressed in Equation 4. Here, E is the total maximum energy provided to the system (pump pulse), and E_0 is the difference in energy between the zero-point energy (ZPE) of the reactant and transition state.

$$k(E) = \frac{G(E - E_0)}{h \cdot N(E)} \qquad (4)$$

The reactant species was taken to be the electronic ground state $I^-\cdot U$ configuration. Calculations by Takayanagi and co-workers[31] find that dissociation of $I^-\cdot U$ clusters to I^- + U proceeds without an exit barrier with a reaction endothermicity of 0.97 eV, calculated at the CAM-B3LYP/aug-cc-pVDZ+α(H:2*s*2*p*) level of theory. Since this barrierless potential does not have a distinct transition state on the potential energy curve (Fig. S4), we employed a variational transition state theory approach[46] by calculating the rate constants along the reaction path to locate the transition state that gave the minimum rate constant. The dissociation potential energy curve was calculated by selecting the I-N1 distance as the reaction coordinate (Fig. S4). Geometry optimizations and vibrational frequency calculations were performed at each I-N1 distance from 2 Å to 20 Å at increments of 0.25 Å and at increments of 0.05~0.1 Å near the transition state. All geometry optimizations and frequency calculations were performed at the MP2/aug-cc-pVDZ(-pp) level of theory. The energy barrier E_0 was calculated as the ZPE-corrected energy difference between the reactant $I^-\cdot U$ and the transition state $[I^-\cdot U]^‡$. A scaling factor of 0.9615[47] corresponding to the MP2/aug-cc-pVDZ level of theory was used to scale the Gaussian-produced vibrational frequencies to account for anharmonicities. To capture the transition state variationally, the rate coefficient for each reactant $I^-\cdot U$ and transition state $[I^-\cdot U]^‡$ pair was calculated using Equation 4 to determine the transition state that yielded a minimum value for the rate constant. The sum and density of states were calculated by implementing the Beyer-Swinehart direct count algorithm with the Stein-Rabinovitch modification[48] for the sum and density of states from the vibrational and rotational frequencies of each species, including explicit treatment for hindered internal rotors.[49] The barrier height and symmetry for hindered internal rotors were calculated by

performing relaxed potential energy scans in Gaussian 09 at the MP2/aug-cc-pVDZ level across the rotational movement in increments of 10°.

As shown in Fig. S5, the dissociation rate constant declines when the I-N1 distance is smaller than 9 Å and increases when the I-N1 distance is greater than 9 Å, so the transition state structure used was the optimized geometry for when I-N1 is 9 Å (Fig. S4). At an I-N1 distance of 9 Å, the calculated barrier height from $I^-\cdot U$ to $[I^-\cdot U]^‡$ was found to be 0.943 eV, and the ZPE-corrected barrier height, or reaction energy was calculated to be 0.947 eV. The total reaction endothermicity was calculated to be 1.10 eV (CCSD). Treating all frequencies harmonically produces an RRKM calculated time constant of 5.3 ps and 2.8 ps for the two excitation energy regions, smaller than the experimental values of 86 ps and 36 ps, respectively. The frequencies of the $I^-\cdots U$ (Table S1) in-plane rocking mode and out-of-plane twisting mode drop dramatically with increasing $I^-\cdots U$ distance and are better treated as hindered rotors in the RRKM analysis. Calculated sums and densities of states for the reactant and transition state species are listed in Table S2. When the $I^-\cdot U$ binary cluster is excited at a photon energy 4.03 eV, i.e. 3.08 eV above the ZPE-corrected reaction energy of 0.947 eV, the RRKM calculated life time is 8.6 ps. At 4.72 eV, i.e. an excess energy of 3.77 eV, the RRKM calculated life time is 4.4 ps. The calculated lifetimes are about a factor of ten shorter than the experimental results of 86 ± 7 ps and 36 ± 3 ps. However, this result approximately reproduces the ratio of the experimental lifetimes at the two pump energies.

V. DISCUSSION

According to the photofragment action spectra (Fig. 1), I^- and $[U-H]^-$ production exhibits maxima around 4.0 eV and 4.8 eV. EOM-CCSD calculations (Table 1) show that $I^-\cdot U$ has two intense resonant excitation regimes which, when shifted by -0.52 eV, line up reasonably well with the experimental maxima. The transitions near 4.0 eV correspond to excitation from the anion ground state to the DBS by promotion of an electron from the I(*5p*) orbital to the DB orbital (*DBO*). Near 4.8 eV, the π-π* transition, localized on the uracil moiety, is dominant and there are considerably weaker transitions representing excitations from I(*5p*) orbitals to a σ* orbital on the nucleobase. Excitation from I(*5p*) orbitals to the π* orbital on the uracil yields excitation energies around 4.5 eV, and the oscillator strengths for these I(*5p*)-π* excitation channels are near zero so the minimum resonant excitation is expected around 4.5 eV. It thus appears that the two maxima in the photofragment action spectra correspond to two very different electronic excitations, one of which leaves neutral iodine complexed to a DB state of U^-, while the other produces I^- complexed to electronically excited uracil. Nonetheless, both final states fragment primarily to I^- with $[U-H]^-$ as a minor channel.

The time-resolved experiment shows the production of I^- at both 4.03 eV and 4.72 eV excitation energies, exhibiting a slow mono-exponential rise in both cases. The fitted rise time constants are fairly long (86 ps and 36 ps, respectively), indicating that statistical decay is likely occurring in both energy regimes. Although the statistical RRKM simulated rise times of 8.6 ps and 4.4 ps underestimate the experimental time constants by an order of magnitude, it roughly reproduces the ratio of the experimental lifetimes at the two pump energies. This discrepancy is likely due to the nature of the loose transition state, and statistical dissociation appears to be the most reasonable option, provided that one can propose sensible mechanisms by which the two very different excited states can relax to form vibrationally excited I^-U in its ground electronic state.

At 4.72 eV, it is quite straightforward to put forth such a mechanism. Our calculations indicate that when the $I^-\cdot U$ binary cluster is excited at 4.72 eV, the π–π* transition of uracil dominates. This π–π* transition produces an excited state with an electronic configuration of $I^-(5p^6)U(\pi^3\pi^{*1})$. Internal conversion could occur from this π–π* excited state to the ground state configuration $I^-(5p^6)U(\pi^4\pi^{*0})$, *i.e.* the electron in the π* anti-bonding orbital falls back to the π orbital in the electronic ground state. Experiments on gas phase uracil have shown the internal conversion following π–π* excitation could occur within ~1 ps,[50-53] leaving uracil in a vibrationally excited electronic ground state, and one expects a similar time constant in I^-U. Upon internal conversion, the highly vibrationally excited cluster can evaporate iodide, whose presence is readily seen in our TRPEI experiment. While it would be desirable to detect decay of the hot I^-U as it dissociates to I^- + U, the VDE of this complex is likely to be similar to that of the cold complex (4.11 eV), which is considerably higher than the probe photon energy. The overall proposed mechanism is given by Equation 5.

$$I^-\cdot U \xrightarrow{h\nu_{pump}} I^-\cdot U(\pi^3\pi^{*1}) \xrightarrow{Internal\ Conversion} I^-\cdot U \rightarrow I^- + U \qquad (5)$$

The assignment of the band at 4.03 eV as photoexcitation to a complex with an electronic configuration of $I(5p^5)U^-(DBO^1)$ is consistent with our earlier time-resolved experiments[21] that showed formation of a complexed DB state ($I\cdot U^-_{DBS}$) of the uracil anion in this energy range. These experiments also revealed that a complexed VB state ($I\cdot U^-_{VBS}$) was formed with a slight delay relative to the DB state; this observation was tentatively attributed to partial conversion of the DB state to the VB state. Regardless, in order for I^- to be a decay product, there needs to be back-transfer of the excess electron from the nucleobase to the iodine, forming hot I^-U that can then dissociate. The overall mechanisms are then represented by Equations 6-8:

$$I^- \cdot U \xrightarrow{h\nu_{pump}} I \cdot U^-_{DBS}, I \cdot U^-_{VBS} \quad (6)$$

$$I \cdot U^-_{DBS} \xrightarrow[Conversion]{Internal} I^- \cdot U \rightarrow I^- + U \quad (7)$$

$$I \cdot U^-_{VBS} \xrightarrow[Conversion]{Internal} I^- \cdot U \rightarrow I^- + U \quad (8)$$

Intuitively, this process might seem more facile from the VB state, given the considerable size mismatch between the DB and I(*5p*) orbitals. Experimentally, there is evidence for back-transfer (i.e. fragmentation to I^-) in photoexcited $I^-(CH_3NO_2)$ complexes,[54] in which the initially formed $I{\cdot}CH_3NO_2^-$ DB state converts within 250 fs to a $I{\cdot}CH_3NO_2^-$ VB state,[27] but not in photoexcited I^-CH_3CN where no such conversion to a VB state occurs.[55] Based on these considerations, Equation 8 is likelier route to I^- production than Equation 7.

Our previous time-resolved experiments[21] showed that at a pump energy of 4.00 eV, signals associated with $I{\cdot}U^-_{DBS}$ and $I{\cdot}U^-_{VBS}$ exhibited biexponential decay with time constants of 8.5 and 200 ps for the DB complex and 16 and 460 ps for the VB complex. The fast decays in both cases were attributed to autodetachment from the complex, but since both fast time constants are considerably shorter than the I^- appearance time of 86 ps, it is possible that they represent back-transfer to form vibrationally hot I^-U, which then dissociates, particularly in the case of the VB complex.

In comparing the results obtained here around 4.7 eV to our earlier time-resolved experiments in this energy range, it is important to understand whether one or two photoexcitation channels are operative. The results here clearly show that π-π* excitation leads to fragmentation to I^-. Our previous results using pump energies from 4.6-4.9 eV and a 790 nm probe pulse indicated prompt formation of an $I{\cdot}U^-_{VBS}$ complex whose lifetime with respect to autodetachment is 410 fs.[19, 21] We attributed formation of this complex to capture of the electron photodetached from the

I^- into the empty π* orbital on the uracil, essentially a two-step process as opposed to direct optical excitation into the π^*; the latter is indeed shown to be very weak in the EOM-CCSD results in Table 1. Nonetheless, as pointed out in our first paper in this series,[19] it is possible to form the $I{\cdot}U^-_{VBS}$ complex via Equation 9:

$$I^-U \xrightarrow{h\nu_{pump}} I^-U^*(\pi^3\pi^*) \rightarrow I \cdot U^-_{VBS} \quad (9)$$

Here, π-π^* excitation on the uracil is followed by electron transfer from the iodide into the empty π orbital. This mechanism is appealing because it implies that only a single photoexcitation process occurs around 4.7 eV. However, the instantaneous appearance of the $I{\cdot}U^-_{VBS}$ complex means that the electron transfer step would have to be exceedingly fast, i.e. less than 50 fs. While this cannot be ruled out, it seems unlikely given the negligible spatial overlap between the HOMO on the I^- and the π MO on the uracil. Moreover, autodetachment signal characteristic of the $I{\cdot}U^-_{VBS}$ complex remains strong out to 5.3 eV, well beyond the π-π* band in Fig. 1b. It would thus appear that two photoexcitation pathways are operative around 4.7 eV, but a more quantitative theoretical treatment is needed to sort out this issue.

VI. CONCLUSIONS

Photofragment action spectroscopy and femtosecond time-resolved photoelectron imaging are utilized to probe the dissociation channels in the $I^-{\cdot}U$ binary complex upon photoexcitation. The photofragment action spectra show both I^- and $[U\text{-}H]^-$ ion signal upon photoexcitation, with $I^-{\cdot}U \rightarrow I^- + U$ as the dominant dissociation channel. The action spectra show two bands for I^- and $[U\text{-}H]^-$ production, with band maxima located at 4.0 eV and 4.8 eV. With the aid of electronic

structure calculations, these bands are assigned, respectively, to excitation of a dipole-bound state of the complex and π-π* excitation of the uracil moiety.

The $I^- \cdot U \rightarrow I^- + U$ is channel is observed in TRPES via photodetachment of the I^- product. Time-resolved experiments are reported at excitation energies of at 4.03 eV and 4.72 eV, where the I^- signal exhibits rise times of 86 ± 7 ps and 36 ± 3 ps, respectively. These long lifetimes are suggestive of internal conversion to the I^-U ground state followed by statistical dissociation, a hypothesis tested by carrying out RRKM calculations of the dissociation rate. At 4.72 eV, internal conversion is likely associated with rapid electronic relaxation of the uracil following π-π* excitation. At. 4.03 eV, there must be back-transfer of a dipole- or valence-bound electron back to the iodine atom, with the latter being more likely. The $I^- \cdot U \rightarrow HI + [U\text{-}H]^-$ channel is not observed in the time-resolved experiments, most likely as a result of low $[U\text{-}H]^-$ production efficiency and a low photodetachment cross section.

ACKNOWLEDGEMENTS

The work described in this paper was funded by the National Science Foundation under Grant No. CHE-1361412. A.K. gratefully acknowledges that this research was conducted with Government support under and awarded by DoD, Air Force Office of Scientific Research, National Defense Science and Engineering Graduate (NDSEG) Fellowship, 32 CFR 168a. CEHD acknowledges support from the European Research Council grant 208589-BIOIONS, the STFC for the provision of equipment from the EPSRC Laser Loan Pool (Grant # 13250030), and the University of York

and Department of Chemistry at the University of York for provision of funds for the Horizon OPO laser system.

References

1. C. von Sonntag, *The Chemical Basis of Radiation Biology*. (Taylor and Francis, London, 1987).
2. K. Aflatooni, G. A. Gallup and P. D. Burrow, J. Phys. Chem. A **102**, 6205 (1998).
3. M. A. Huels, I. Hahndorf, E. Illenberger and L. Sanche, J. Chem. Phys. **108**, 1309 (1998).
4. B. Boudaiffa, P. Cloutier, D. Hunting, M. A. Huels and L. Sanche, Science **287**, 1658 (2000).
5. M. A. Huels, B. Boudaiffa, P. Cloutier, D. Hunting and L. Sanche, J. Am. Chem. Soc. **125**, 4467 (2003).
6. G. Hanel, B. Gstir, S. Denifl, P. Scheier, M. Probst, B. Farizon, M. Farizon, E. Illenberger and T. D. Mark, Phys. Rev. Lett. **90**, 188104 (2003).
7. S. Denifl, S. Ptasinska, M. Probst, J. Hrusak, P. Scheier and T. D. Mark, J. Phys. Chem. A **108**, 6562 (2004).
8. F. Martin, P. D. Burrow, Z. L. Cai, P. Cloutier, D. Hunting and L. Sanche, Phys. Rev. Lett. **93**, 068101 (2004).
9. L. Sanche, Eur. Phys. J. D **35**, 367 (2005).
10. D. Huber, M. Beikircher, S. Denifl, F. Zappa, S. Matejcik, A. Bacher, V. Grill, T. D. Maerk and P. Scheier, J. Chem. Phys. **125**, 084304 (2006).
11. L. Sanche, Nature **461**, 358 (2009).
12. C.-R. Wang, J. Nguyen and Q.-B. Lu, J. Am. Chem. Soc. **131**, 11320 (2009).
13. J. Simons, Accounts Chem. Res. **39**, 772 (2006).
14. J. D. Gu, Y. M. Xie and H. F. Schaefer, J. Am. Chem. Soc. **128**, 1250 (2006).
15. H.-Y. Chen, P.-Y. Yang, H.-F. Chen, C.-L. Kao and L.-W. Liao, J. Phys. Chem. B **118**, 11137 (2014).
16. X. Pan and L. Sanche, Chem. Phys. Lett. **421**, 404 (2006).
17. J. Gu, J. Leszczynski and H. F. I. Schaefer, Chem. Rev. **112**, 5603 (2012).

18. A. M. Scheer, C. Silvernail, J. A. Belot, K. Aflatooni, G. A. Gallup and P. D. Burrow, Chem. Phys. Lett. **411**, 46 (2005).
19. M. A. Yandell, S. B. King and D. M. Neumark, J. Am. Chem. Soc. **135**, 2128 (2013).
20. S. B. King, M. A. Yandell and D. M. Neumark, Faraday Discuss. **163**, 59 (2013).
21. S. B. King, M. A. Yandell, A. B. Stephansen and D. M. Neumark, J. Chem. Phys. **141**, 224310 (2014).
22. S. B. King, A. B. Stephansen, Y. Yokoi, M. A. Yandell, A. Kunin, T. Takayanagi and D. M. Neumark, J. Chem. Phys. **143** (2015).
23. A. B. Stephansen, S. B. King, Y. Yokoi, Y. Minoshima, W. L. Li, A. Kunin, T. Takayanagi and D. M. Neumark, J. Chem. Phys. **143**, 104308 (2015).
24. J. H. Hendricks, S. A. Lyapustina, H. L. de Clercq, J. T. Snodgrass and K. H. Bowen, J. Chem. Phys. **104**, 7788 (1996).
25. J. Schiedt, R. Weinkauf, D. M. Neumark and E. W. Schlag, Chem. Phys. **239**, 511 (1998).
26. R. A. Bachorz, W. Klopper, M. Gutowski, X. Li and K. H. Bowen, J. Chem. Phys. **129**, 054309 (2008).
27. M. A. Yandell, S. B. King and D. M. Neumark, J. Chem. Phys. **140**, 184317 (2014).
28. T. Sommerfeld, J. Phys. Chem. A **108**, 9150 (2004).
29. T. Takayanagi, T. Asakura and H. Motegi, J. Phys. Chem. A **113**, 4795 (2009).
30. H. Motegi and T. Takayanagi, J. Mol. Struct. **907**, 85 (2009).
31. Y. Yokoi, K. Kano, Y. Minoshima and T. Takayanagi, Comput. Theor. Chem. **1046**, 99 (2014).
32. R. J. Peláez, C. Blondel, C. Delsart and C. Drag, J. Phys. B-At. Mol. Opt. **42**, 125001 (2009).
33. H.-T. Liu, C.-G. Ning, D.-L. Huang and L.-S. Wang, Angew. Chem. Int. Ed. **53**, 2464 (2014).
34. A. Sen, T. F. M. Luxford, N. Yoshikawa and C. E. H. Dessent, Phys. Chem. Chem. Phys. **16**, 15490 (2014).
35. A. Sen and C. E. H. Dessent, J. Chem. Phys. **141**, 241101 (2014).
36. A. V. Davis, R. Wester, A. E. Bragg and D. M. Neumark, J. Chem. Phys. **118**, 999 (2003).

37. A. E. Bragg, J. R. R. Verlet, A. Kammrath, O. Cheshnovsky and D. M. Neumark, J. Am. Chem. Soc. **127**, 15283 (2005).

38. V. Dribinski, A. Ossadtchi, V. A. Mandelshtam and H. Reisler, Rev. Sci. Instrum. **73**, 2634 (2002).

39. *See supplementary material at http://dx.doi.org/* .

40. R. A. Kendall, T. H. Dunning and R. J. Harrison, J. Chem. Phys. **96**, 6796 (1992).

41. K. A. Peterson, D. Figgen, E. Goll, H. Stoll and M. Dolg, J. Chem. Phys. **119**, 11113 (2003).

42. K. A. Peterson, B. C. Shepler, D. Figgen and H. Stoll, J. Phys. Chem. A **110**, 13877 (2006).

43. M. J. Frisch, G. W. Trucks, H. B. Schlegel and *et. al.*, GAUSSIAN 09, Gaussian Inc, Wallingford, CT, USA, 2009.

44. T. Baer and W. L. Hase, *Unimolecular Reaction Dynamics: Theory and Dynamics*. (Oxford University Press, USA, New York, 1996).

45. R. G. Gilbert and S. C. Smith, *Theory of Unimolecular and Recombination Reactions*. (Blackwell Scientific Publications, London, 1990).

46. J. I. Steinfeld, J. S. Francisco and W. L. Hase, *Chemical Kinetics and Dynamics*. (Prentice-Hall, New Jersey, 1999).

47. J. P. Merrick, D. Moran and L. Radom, J. Phys. Chem. A **111**, 11683 (2007).

48. S. E. Stein and B. S. Rabinovitch, J. Chem. Phys. **58**, 2438 (1973).

49. T. Beyer and D. F. Swinehart, Commun. Acm **16**, 379 (1973).

50. S. Ullrich, T. Schultz, M. Z. Zgierski and A. Stolow, Phys. Chem. Chem. Phys. **6**, 2796 (2004).

51. C. Canuel, M. Mons, F. Piuzzi, B. Tardivel, I. Dimicoli and M. Elhanine, J Chem Phys **122**, 074316 (2005).

52. H. Kang, K. T. Lee, B. Jung, Y. J. Ko and S. K. Kim, J. Am. Chem. Soc. **124**, 12958 (2002).

53. S. Matsika, J. Phys. Chem. A **108**, 7584 (2004).

54. C. E. H. Dessent, J. Kim and M. A. Johnson, Faraday Disc. **115**, 395 (2000).

55. C. E. H. Dessent, C. G. Bailey and M. A. Johnson, J. Chem. Phys. **103**, 2006 (1995).

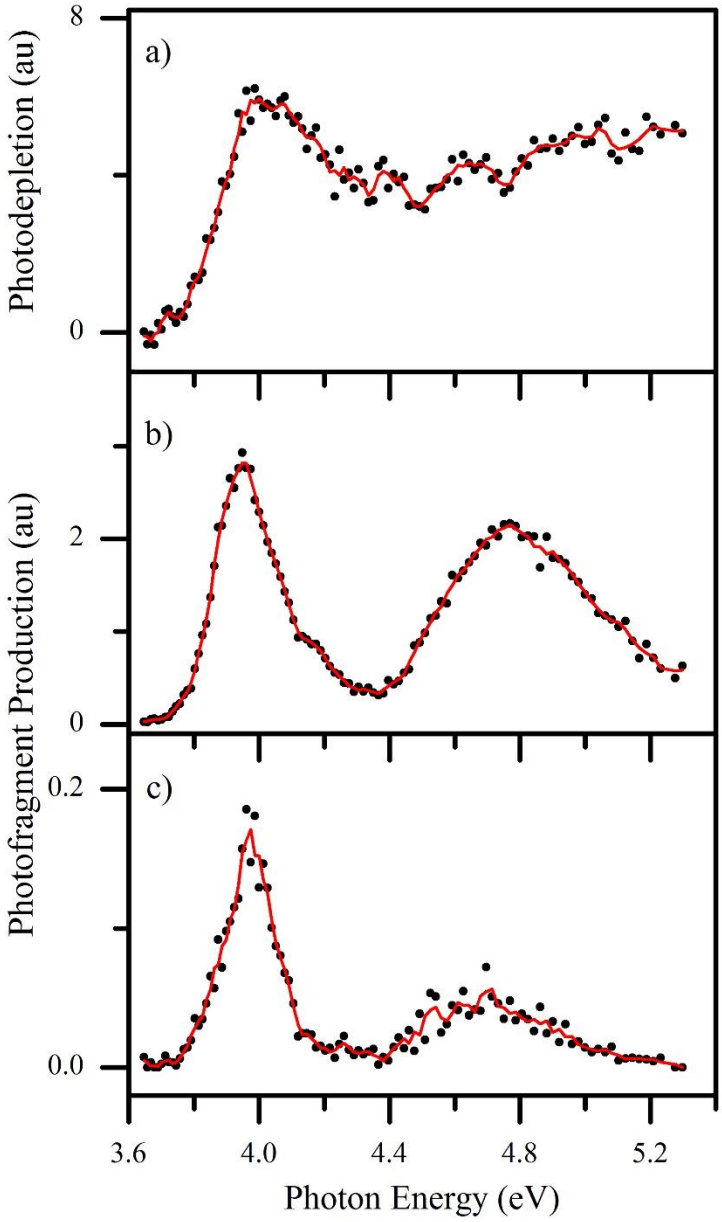

FIG 1. a) Photodepletion (absorption) spectrum of $I^-{\cdot}U$ displayed with the corresponding photofragment action spectra of the (b) I^- and (c) $[U\text{-}H]^-$ photofragments. The solid lines represent 3 point smooths through the data points.

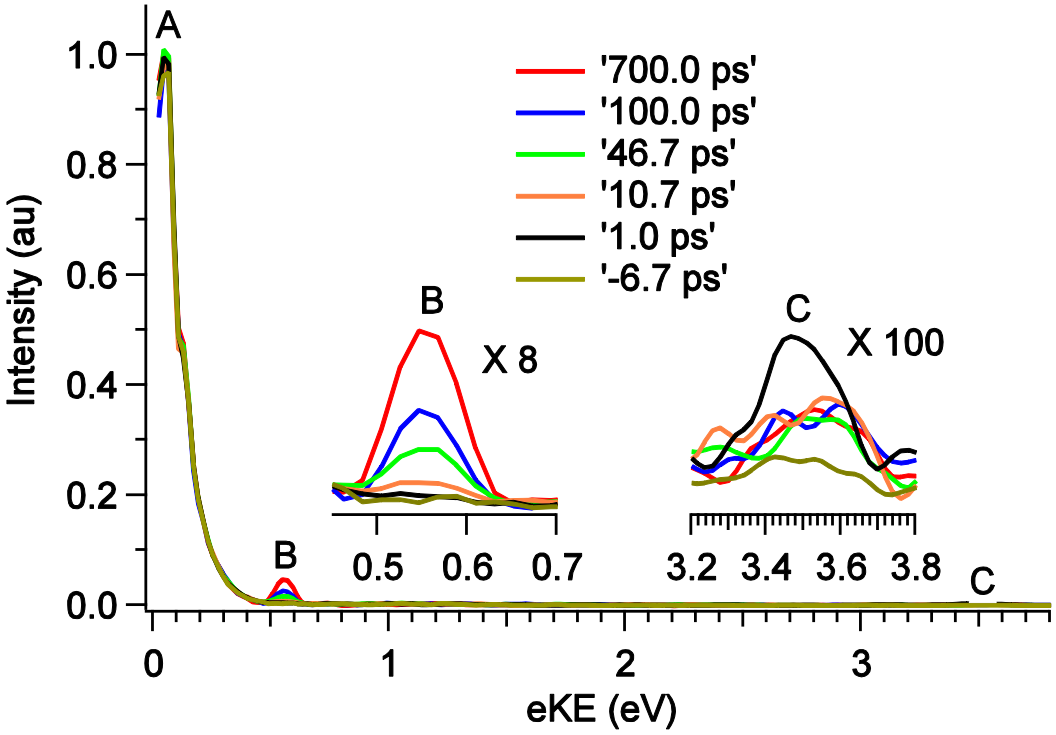

FIG 2. Photoelectron spectrum of $I^{-}\cdot U$ species at 4.03 eV pump and 3.61 eV probe at selected delay times.

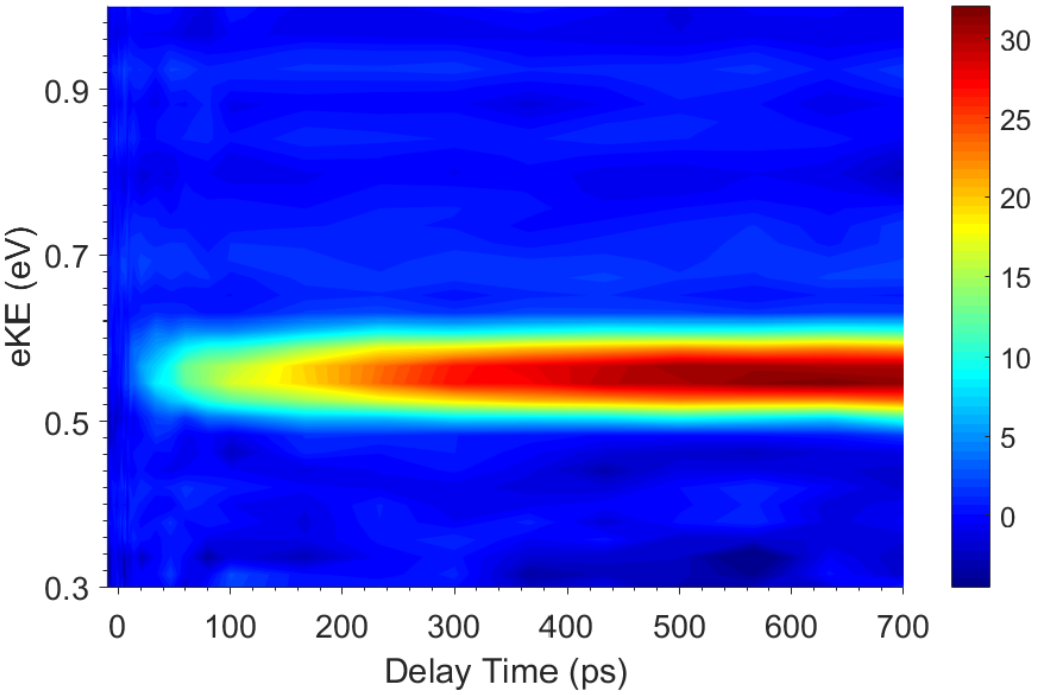

FIG 3. Time-resolved photoelectron spectra for feature B at pump-probe delays for $I^{-}\cdot U$ at excitation energy of 4.03 eV (near the VDE) and probe energy of 3.61 eV.

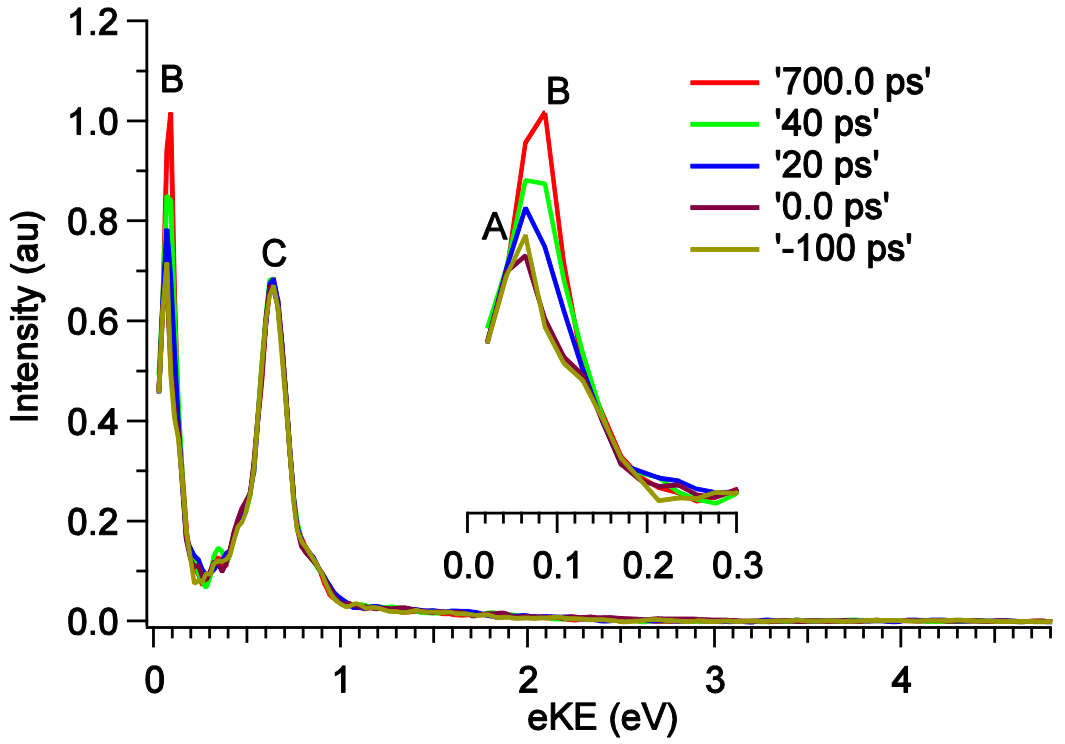

FIG 4. Photoelectron spectrum of $I^{-}\cdot U$ species with 4.72 eV pump (significantly above the VDE) and 3.15 eV probe at selected delay times.

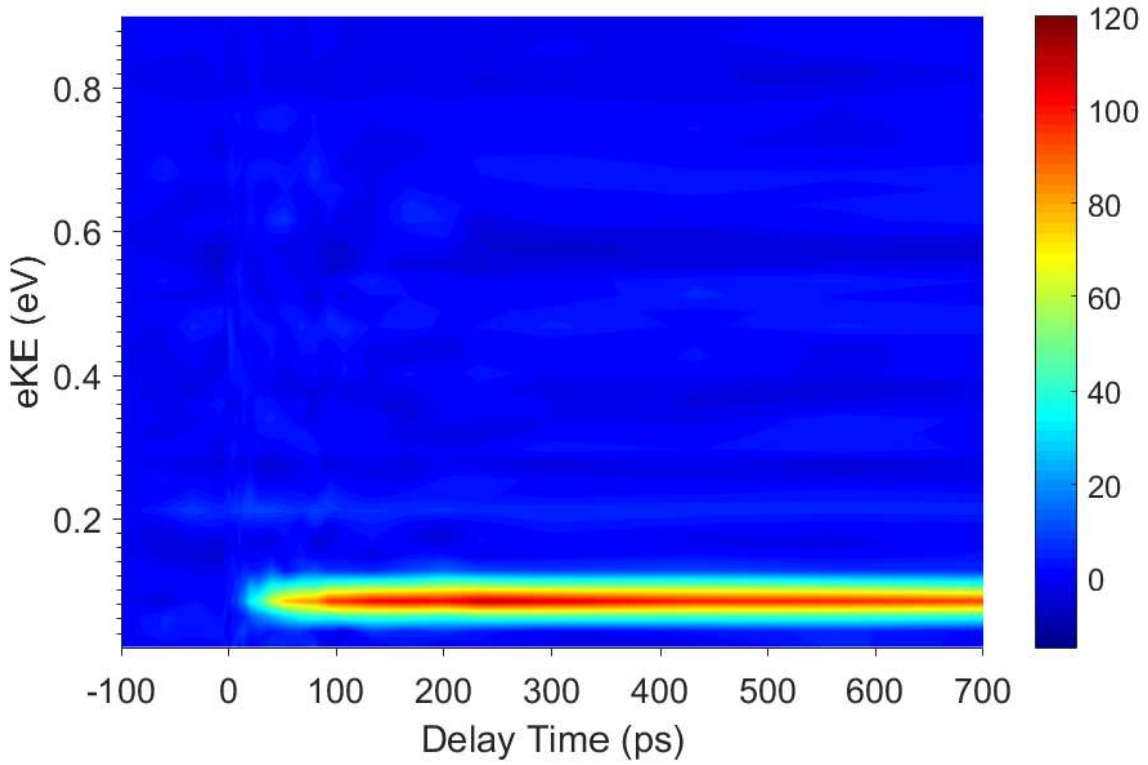

FIG 5 Time-resolved photoelectron spectrum for feature B at pump-probe delays for $I^{-}\cdot U$ with an excitation energy of 4.72 eV and probe energy of 3.15 eV.

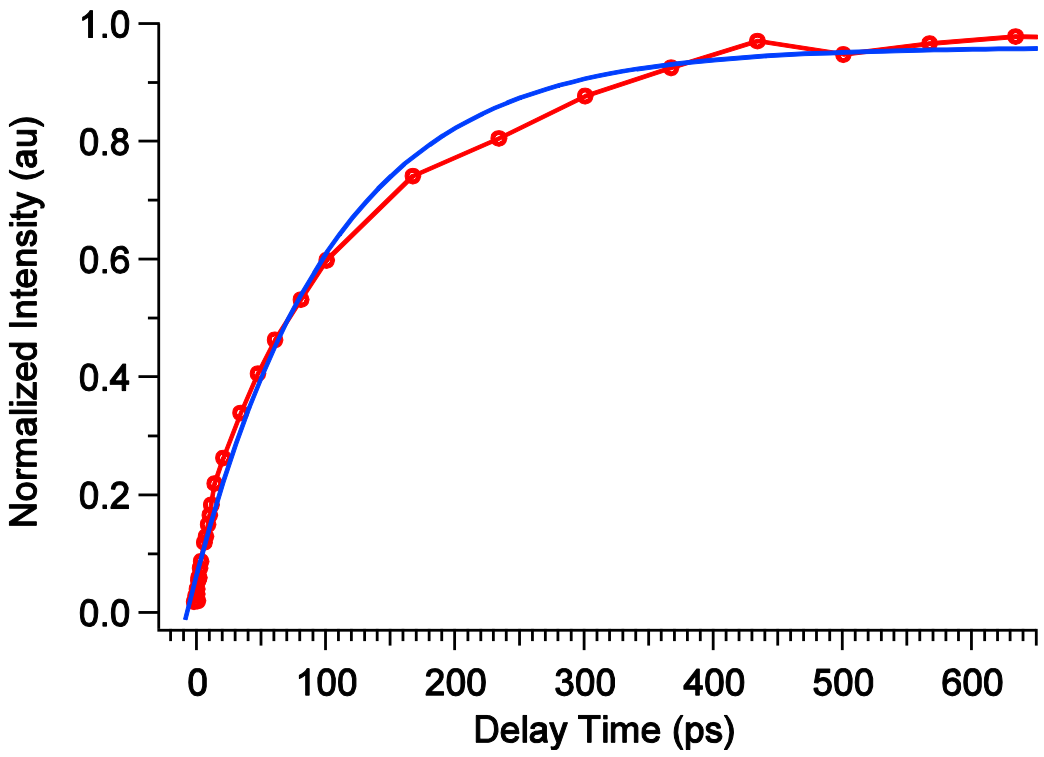

FIG 6. Integrated intensity of feature B from excitation at 4.30 eV vs, delay time. The rise time for feature B is 86 ± 7 ps.

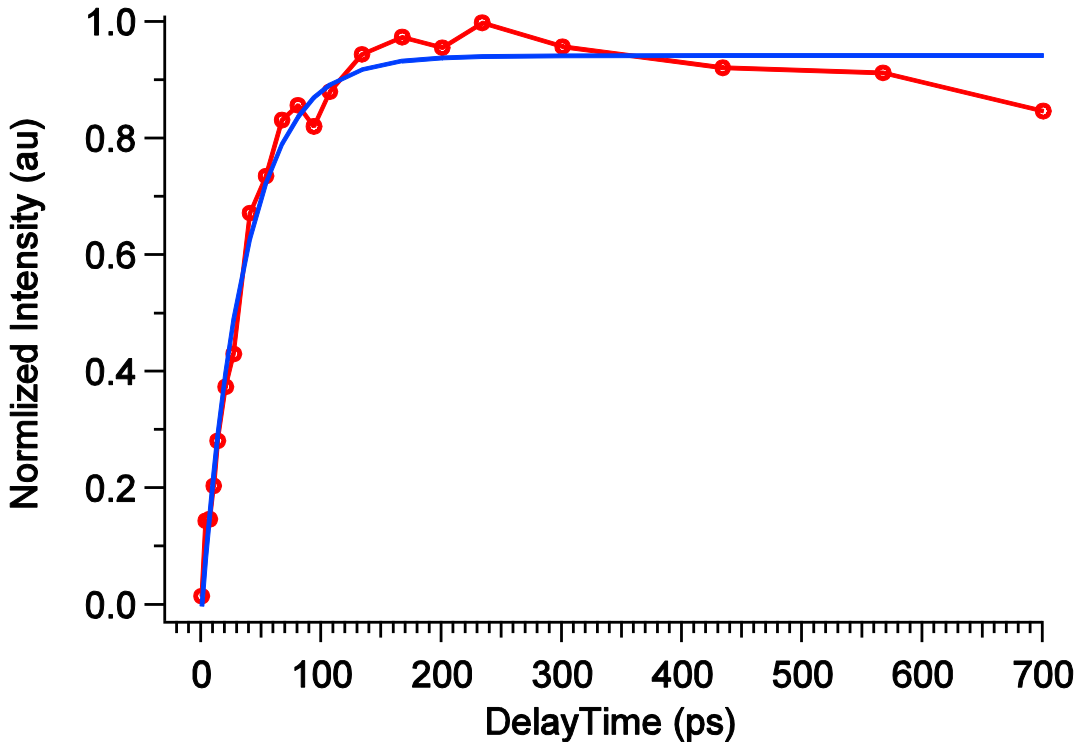

FIG 7. Integrated intensities of feature B from excitation at 4.72 eV vs. delay time. The rise-time for feature B is 36 ± 3 ps.

SUPPLEMENTARY MATERIAL

Photodissociation dynamics of the iodide-uracil (I^-U) complex

Wei-Li Li[1], Alice Kunin[1], Edward Matthews[2], Naruo Yoshikawa,[2] Caroline E. H. Dessent[2], Daniel M. Neumark[1,3,*]

[1]Department of Chemistry, University of California, Berkeley, CA 94720, USA.

[2]Deparment of Chemistry, University of York, Heslington, York, YO10 5DD, UK.

[3]Chemical Sciences Division, Lawrence Berkeley National Laboratory, Berkeley, CA 94702, USA

E-mail: dneumark@berkeley.edu, caroline.dessent@york.ac.uk

Table S1. Vibrational frequencies (cm^{-1}) of $I^-\cdot U$ ground state, transition and bare neutral uracil at MP2/aug-cc-pVDZ(-pp) level of theory.

$I^-\cdot U$ ground state				$I^-\cdot U$ transition state				Uracil neutral		
54.9	57.8	97.0		-8.9	11.8	23.0				
154.1	183.3	380.1		144.4	165.5	380.5		142.3	160.9	381.0
425.1	515.3	537.8		397.2	512.3	533.2		389.0	510.9	532.3
561.0	677.4	724.4		552.8	579.6	685.4		551.9	561.9	689.3
751.5	778.3	799.7		724.5	743.6	770.7		720.7	742.0	769.3
840.5	973.8	984.8		810.1	954.0	973.7		805.1	941.0	970.8
998.2	1090.6	1213.8		985.0	1085.9	1206.6		983.8	1085.5	1202.6
1232.2	1369.9	1386.9		1241.1	1381.4	1401.3		1241.7	1383.5	1398.7
1414.9	1518.0	1658.8		1418.9	1501.6	1667.6		1415.8	1503.1	1669.2
1730.4	1763.4	3218.3		1750.9	1782.4	3246.9		1754.0	1788.0	3247.7
3222.7	3276.8	3607.8		3284.8	3599.8	3640.7		3284.5	3592.7	3644.7

Table S2. Beyer-Swinehart calculated densities and sums of states for the $I^-\cdot U$ ground state and transition state including treatment of low-frequency hindered internal rotational modes.

Excitation Energy (eV)	$I^-\cdot U$ ground state density ($/cm^{-1}$)	$I^-\cdot U$ transition state sum	$k_{RRKM}(E)$ (1/s)	Lifetime (ps)
4.03	3.75466×10^{15}	1.45548×10^{16}	1.16213×10^{11}	8.6
4.72	1.00448×10^{17}	7.61756×10^{17}	2.27349×10^{11}	4.4

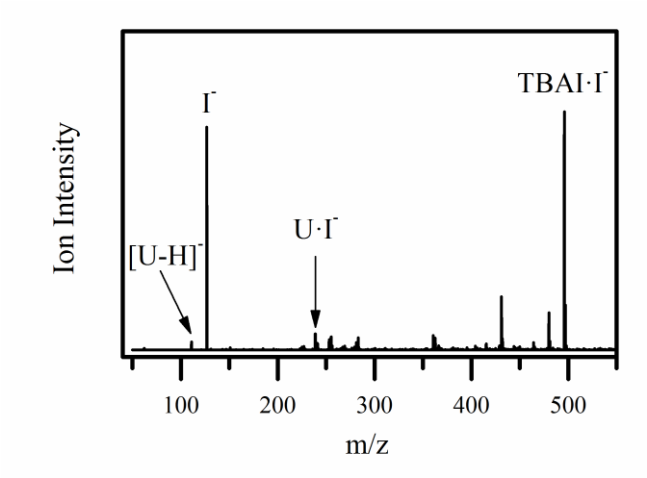

Figure S1: Negative ion ESI-MS of an iodide/uracil solution.

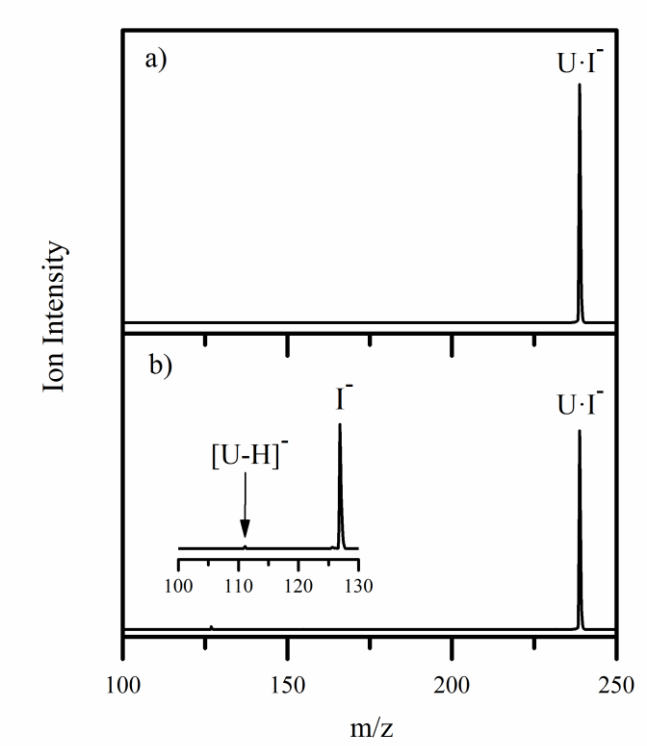

Figure S2: a) Isolation of the I^{-}·U cluster prior to laser irradiation, and b) photofragmentation mass spectrum of I^{-}·U obtained at 260 nm (4.78 eV) showing production of I- as the dominant photofragment and $[U-H]^{-}$ as a minor photofragment.

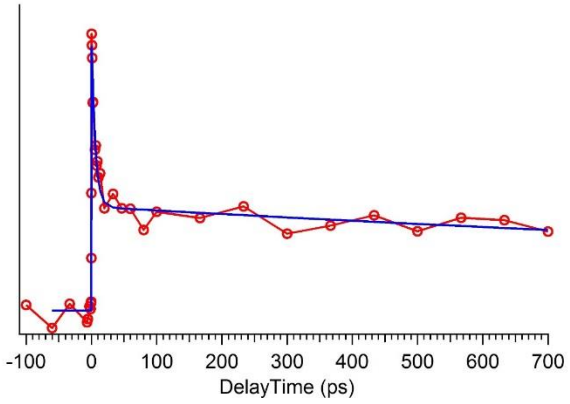

Figure S3: Time-resolved photoelectron spectrum for feature C at pump-probe delays for $I^{-}\cdot U$ with an excitation energy of 4.03 eV and probe energy of 3.61 eV. The rise time constant is 0.3 ps, the decay time contestant are 6 ps and 2800 ps.

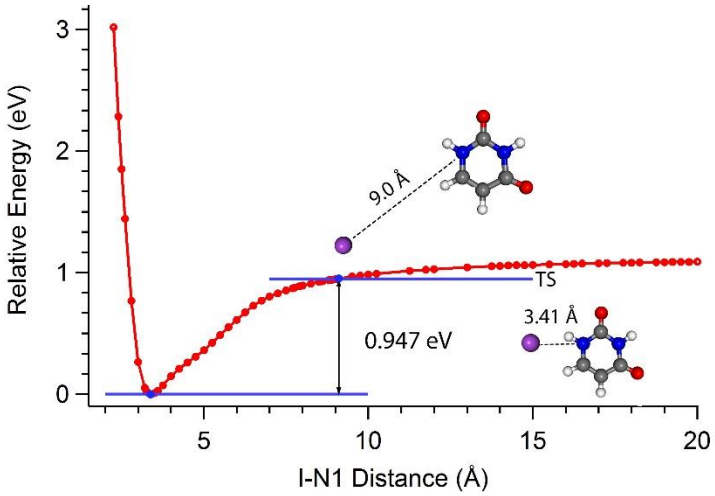

Figure S4: Potential Energy Curve calculated by geometry optimization at frozen I-N1 distances. The calculations are performed at MP2/aug-cc-pvDZ-(pp) level of theory. All energies are ZPE corrected.

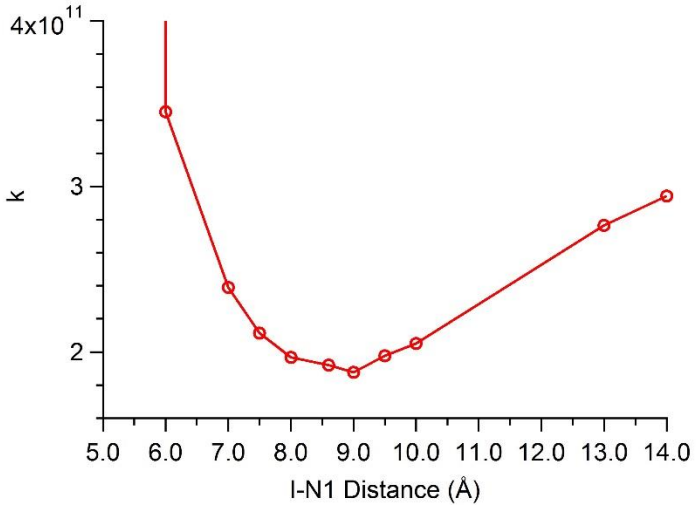

Figure S5: the dissociation rate constant at I-N1 distances from 6 to 14 Å.